Available online at www.sciencedirect.com
SCIENCE DIRECT®
Physics of the Earth and Planetary Interiors 140 (2003) 73–89
PHYSICS OF THE EARTH AND PLANETARY INTERIORS
www.elsevier.com/locate/pepi

Continuous global geomagnetic field models for the past 3000 years

Monika Korte [a,b], Catherine Constable [b]

[a] *GeoForschungsZentrum Potsdam, Telegrafenberg, 14473 Potsdam, Germany*
[b] *Institute for Geophysics and Planetary Physics, Scripps Institution of Oceanography, University of California, San Diego, 9500 Gilman Drive, La Jolla, CA 92093-0225, USA*

Accepted 11 July 2003

Abstract

Several global geomagnetic field models exist for recent decades, but due to limited data availability models for several centuries to millennia are rare. We present a continuous spherical harmonic model for almost 3 millennia from 1000 B.C. to 1800 A.D., based on a dataset of directional archaeo- and paleomagnetic data and axial dipole constraints. The model, named Continuous Archaeomagnetic and Lake Sediment Geomagnetic Model for the last 3k years (CALS3K.1), can be used to predict both the field and secular variation. Comparisons and tests with synthetic data lead to the conclusion that CALS3K.1 gives a good general, large-scale representation of the geomagnetic field, but lacks small-scale structure due to the limited resolution of the sparse dataset. In future applications the model can be used for comparisons with additional, new data for that time span. For better resolved regions, the agreement of data with CALS3K.1 will provide an idea about the general compatibility of the data with the field and secular variation in that region of the world. For poorly covered regions and time intervals we hope to iteratively improve the model by comparisons with and inclusion of new data. Animations and additional snapshot plots of model predictions as well as the model coefficients and a FORTRAN code to evaluate them for any time can be accessed under http://www.mahi.ucsd.edu/cathy/Holocene/holocene.html. The whole package is also stored in the Earthref digital archive at http://www.earthref.org/...

Keywords: Geomagnetic field modelling; Secular variation; Archaeomagnetism; Paleomagnetism; Geodynamo

1. Introduction

Global geomagnetic field models can offer valuable information for improved understanding of the dynamics of the Earth's core. The widely used modelling technique using spherical harmonic basis functions allows, under the assumption of a source free, insulating mantle, the downward continuation of the model obtained from data at or above the Earth's surface to the core-mantle boundary (CMB), the region of origin of the geomagnetic field and its secular variation. Under the frozen-flux hypothesis (Roberts and Scott , 1965) temporal variations in magnetic flux at the CMB can reveal fluid flow patterns. Apparently persistent, stationary flux lobes observed in recent and historical models give rise to theories about thermal (Bloxham and Gubbins , 1987) or topographical (Gubbins and Richards , 1986) coupling of core and mantle.

Systematic measurements of the full vector geomagnetic field, however, exist for less than 200 years, a very short interval compared to the time-scales of secular variation. A whole suite of global models representing the geomagnetic field and its secular

E-mail addresses: monika@gfz-potsdam.de (M. Korte), cconstable@ucsd.edu (C. Constable).

0031-9201/$ – see front matter © 2003 Elsevier B.V. All rights reserved.
doi:10.1016/j.pepi.2003.07.013

variation have been developed for recent decades, like the temporally continuous models GSFC (Sabaka et al. , 1997), CM3 (Sabaka et al. , 2002) or DGRF, a set of individual models adopted every 5 years by International Association of Geomagnetism and Aeronomy (IAGA) Working Group V-8 (e.g. Mandea and Macmillan , 2000), to name just a few. Bloxham and Jackson (1992) covered the time from the beginning of magnetic vector measurements in 1840 with their continuous model UFM1. Jackson et al. (2000) complemented the data with historical measurements of declination and inclination going back as far as the 16th century and developed a continuous model, GUFM, for the past 400 years starting in 1590 A.D.For older times only indirect records of the field from the remanent magnetisation preserved in archaeo- and paleomagnetic samples are available. This kind of data has significantly higher uncertainties than directly measured data: assumptions about the way the magnetisation was acquired are involved (e.g. Merrill et al. , 1996) and in particular the dating of samples is often problematic. Uncertainties on the order of a few years to decades may be realistic for some archaeological artefacts or lava flows, but when radiocarbon dating or similar methods have to be used the uncertainties easily become on the order of centuries (Stuiver and Reimer , 1993; Stuiver et al. , 1998). Therefore, on a global scale time-averaged models over long intervals have been the main objects studied, e.g. by Carlut and Courtillot (1998), Johnson and Constable (1997), Kelly and Gubbins (1997), McElhinny et al. (1996), Schneider and Kent (1990), Hatakeyama and Kono (2002). Only recently were efforts started to extend the non-averaged global models further back in time. Based on archaeomagnetic data compiled by Daly and Goff (1996), Hongre et al. (1998) investigated a low-degree spherical harmonic model of the field over the last 2000 years. Lund and Constable (in preparation) compiled the dataset PSVMOD1.0, a combination of archaeomagnetic and lake sediment paleomagnetic data for the past 3000 years. Johnson and Constable (1998) derived a time-averaged model, ALS3K, from that dataset and global individual 100 year snapshots were modelled by Constable et al. (2000). Those snapshot models show a coherent temporal evolution of the field, but smoothness and misfit of each model had been chosen merely by the expected or desired appearance of the model for some of the epochs. In this paper, we present a temporally continuous model where all epochs of that dataset have been modelled consistently, thus increasing the reliability of structure changing with time and allowing the study of secular variation.

We compare the continuous models to snapshots and to GUFM for the overlapping time interval. An error-analysis and additional tests with synthetic data are used to investigate the reliability of features seen in our model. The structure of a preferred continuous model is briefly discussed with respect to the spatially smoother snapshot models discussed in detail by Constable et al. (2000). Some instantaneous snapshots and averages of the model's secular variation prediction for the radial component are shown and the outlook for planned improvements of the model is given in Section 7.

2. Data

For the continuous models presented here we use PSVMOD1.0 by Lund and Constable (in preparation) as the primary dataset. PSVMOD1.0 has been modelled as 100-year snapshots by Constable et al. (2000). Details of the dataset are given in those two papers, we only summarise some important features here. The data consist of 24 globally distributed time series, 12 of them regionally composite archaeomagnetic series and 12 of them lake sediment paleomagnetic data (Fig. 1). All data are claimed to have independent good quality age control. Where C^{14} dating was used the time-scales were originally transformed to calendar ages using the calibration curve of Clark (1975) and were susbequently checked for consistency with the calibration by Stuiver et al. (1998). The records consist of 100-year interval data, which were obtained by an evaluation of a composite, continuous curve at those times. Each datum represents something like a 20–30 year average of the field. Only directional data, i.e. declination and inclination, are used. Errors were estimated by a comparison of the most recent parts of the data series with the historical UFM model (Bloxham and Jackson , 1992). Standard error values of 2.5° were assigned to both inclination and declination of archaeomagnetic records 3.5 and 5.0°, respectively for inclination and declination of lake sediments (Constable et al. , 2000). Even with good age control,

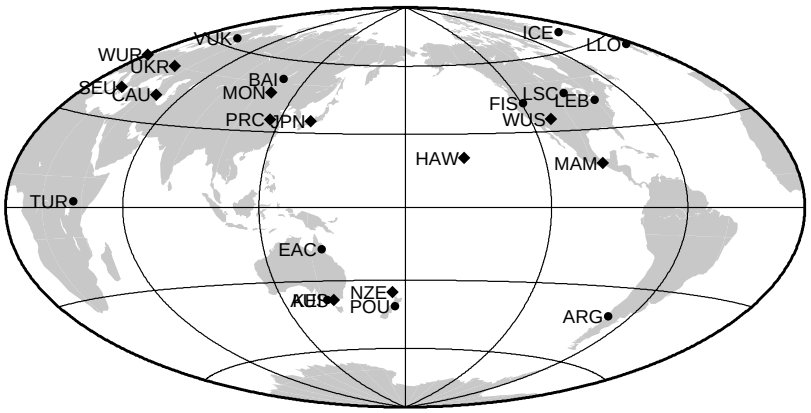

Fig. 1. PSVMOD1.0 sites. Dots have lake sediment data, diamonds archaeomagnetic. Archaeomagnetic site AUS and Lake Keilambete (KEI) in southern Australia are closely adjacent.

however, we have to remember that dating uncertainties are an additional problem in archaeo- and paleomagnetic data compared to recent and historical data. For individual data points dating uncertainties can reach the order of a few hundred years, and smooth time series for sites can be streched or compressed in time by dating uncertainties of the individual points of which they are compiled. Note also the uneven spatial distribution of sites in Fig. 1. With only one site in South America and Africa, respectively, the southern hemisphere is poorly represented. Moreover, the single African record is inclination only and the South American time series only starts at 0 A.D., there are no South American data at all for the earlier millennium. Also the New Zealand archaeomagnetic record only covers the most recent 1000 years and the Australian archaeomagnetic series has a long gap between 0 A.D. and 1000 A.D. The coverage of Asia is worse than that of Europe and North America: The Mongolian archaeomagnetic record is inclination only and goes back no further than 700 A.D., and the Japanese record only covers the time span from 0 to 1800 A.D. In addition to PSVMOD1.0 we used interpolated values of global axial dipole moment to provide an intensity constraint (see Section 3).

3. Modelling method

To develop a time-dependent global model a combined representation in space and in time is necessary. We follow closely the methodology of Bloxham and Jackson (1992) using the conventional spatial expansion in spherical harmonic functions with a temporal expansion in cubic B-spline basis functions $M_n(t)$ as briefly outlined in the following. By adopting the widely used approximation of an insulating mantle, and neglecting crustal fields and external fields the time-dependent geomagnetic field $\boldsymbol{B}(t)$ can be written as the negative gradient of a scalar potential $V(t)$, $\boldsymbol{B}(t) = -\nabla V(t)$ everywhere outside the Earth's core

$$V(r,\theta,\phi,t) = R_{\mathrm{E}} \sum_{l=1}^{l_{\max}} \sum_{m=0}^{l} \sum_{n=1}^{n_{\max}} \left(\frac{R_{\mathrm{E}}}{r}\right)^{l+1} \times [g_l^{m,n} \cos(m\phi) + h_l^{m,n} \sin(m\phi)] P_l^m(\cos\theta) M_n(t) \quad (1)$$

where (r,θ,ϕ) are spherical polar coordinates and $R_{\mathrm{E}} = 6371.2$ km is the mean radius of the Earth's surface. Downward continuation to the CMB is achieved by setting the ratio R_{E}/r to 1.828. The $P_l^m(\cos\theta)$ are the Schmidt quasi-normalised associated Legendre functions of degree l and order m. The coefficients $\{g_l^{m,n}, h_l^{m,n}\}$}are related to the standard time-dependent Gauss coefficients $\{g_l^m, h_l^m\}$ by

$$g_l^m(t) = \sum_{n=1}^{n_{\max}} g_l^{m,n} M_n(t) \quad (2)$$

and the same for h_l^m. Cubic B-splines are piecewise cubic polynomials, which form a basis of minimal support (de Boor , 1978). The ith cubic B-spline M_i

is non-zero ($M_i(t) > 0$) only if t lies in the interval $(t_i, ti + 4)$ of knot points t_n, $n = 1$ to $n_{\max}$.

We use the inverse method based on the work of Whaler and Gubbins (1981) and Gubbins (1983), minimising the function

$$(\gamma - \boldsymbol{fm})^{\mathrm{T}} \boldsymbol{C}_{\mathrm{e}}^{-1} (\gamma - \boldsymbol{fm}) + \boldsymbol{m}^{\mathrm{T}} \boldsymbol{\Lambda} \boldsymbol{m} \tag{3}$$

where $(\gamma - fm)$ is the error vector given by the difference between data γ and the prediction of the model $\boldsymbol{m}$ and $\boldsymbol{f}$ is the operator relating the data vector to the model according to Eq. (1). $\boldsymbol{C}_{\mathrm{e}}$ is the data error covariance matrix and the second term is the regularisation condition, which consists of a spatial and a temporal part:

$$\Lambda = \lambda \boldsymbol{S}^{-1} + \tau \boldsymbol{T}^{-1} \tag{4}$$

with the spatial and temporal damping factors λ and τ, respectively. The operators $\boldsymbol{S}$ and $\boldsymbol{T}$ are diagonal matrices, the elements of which depend on the chosen norm. Like Bloxham and Jackson (1992) for their UFM models we will use the minimum Ohmic heating norm of Gubbins (1975) for the spatial regularisation

$$\begin{aligned} \boldsymbol{m}^{\mathrm{T}} \boldsymbol{S}^{-1} \boldsymbol{m} = {} & \frac{4\pi}{(t_{\mathrm{e}} - t_{\mathrm{s}})} \\ & \times \int_{t_{\mathrm{s}}}^{t_{\mathrm{e}}} \sum_{l=1}^{l_{\max}} \frac{(l+1)(2l+1)(2l+3)}{l} \left(\frac{R_{\mathrm{E}}}{r} \right)^{2l+4} \\ & \times \sum_{m=0}^{l} [(g_l^m)^2 + (h_l^m)^2] \, \mathrm{d}t \end{aligned} \tag{5}$$

and the temporal norm of minimum surface integral of second derivative of the radial field

$$\boldsymbol{m}^{\mathrm{T}} \boldsymbol{T}^{-1} \boldsymbol{m} = \frac{1}{(t_{\mathrm{e}} - t_{\mathrm{s}})} \int_{t_{\mathrm{s}}}^{t_{\mathrm{e}}} \int_{\mathrm{CMB}} (\partial_t^2 B_{\mathrm{r}})^2 \, \mathrm{d}\Omega \, \mathrm{d}t \tag{6}$$

where $(t_{\mathrm{s}}, t_{\mathrm{e}})$ is the time interval over which we solve. Except for the additional time-dependence the method is basically the same as used by Constable et al. (2000) for the individual snapshot models. The measured directional and intensity data are non-linearly related to the coefficients. We therefore have to find the solution iteratively, which we do using the scheme described in detail by Gubbins and Bloxham (1985):

$$\begin{aligned} \boldsymbol{m}_{i+1} = {} & \boldsymbol{m}_i + (\boldsymbol{A}_i^{\mathrm{T}} \boldsymbol{C}_{\mathrm{e}}^{-1} \boldsymbol{A}_i + \boldsymbol{\Lambda})^{-1} \\ & \times [\boldsymbol{A}_i^{\mathrm{T}} \boldsymbol{C}_{\mathrm{e}}^{-1} (\gamma - \boldsymbol{f}(\boldsymbol{m}_i)) - \boldsymbol{\Lambda} \boldsymbol{m}_i] \end{aligned} \tag{7}$$

where $\boldsymbol{m}_i$ is the model at the ith iteration and

$$\boldsymbol{A}_i = \left. \frac{\partial \boldsymbol{f}}{\partial \boldsymbol{m}} \right|_{\boldsymbol{m} = \boldsymbol{m}_i} \tag{8}$$

is the Fréchet derivative at $\boldsymbol{m}_i$. This is a different approach from Occam's iteration process (Constable et al. , 1987; Parker , 1994) used by Constable et al. (2000), but from the comparisons that we did we suppose that the results do not differ significantly in this case.

We choose the maximum degree and order of the spherical harmonic expansion high enough that the roughness of the models is determined only by data and regularisation, not by truncation level. With our maximum of 24 sites we used maximum degree and order 10. (Bloxham and Jackson (1992) use degree and order 14 because they have much better data coverage at least for recent epochs.) Note, however, that this does not mean that we can actually resolve all these coefficients well. Only the lower degree and order coefficients can be resolved with any confidence. The same requirement applies to the number of splines, and that number was chosen as 50. With 3000 years of data this gives knot points every 60 years as opposed to 2.5 years for Bloxham and Jackson (1992) and Jackson et al. (2000).

The directional dataset can determine the field models only to within an arbitrary multiplier due to the lack of intensity information. Hulot et al. (1997) show that this is true if two and only two magnetic poles exist, but conclude that this can generally be taken as a valid assumption for historical or archaeomagnetic data. Constraining the axial dipole coefficient g_1^0 resolves this ambiguity. For their snapshot models Constable et al. (2000) chose to fix g_1^0 to the value of 30 μT, the order of magnitude of the present field. We are, however, planning to eventually supplement the dataset with intensity information, in which case we must not have a completely fixed g_1^0 but might still want to utilise some weaker constraint on it for robustness of the models. Therefore we chose to treat the default values for the g_1^0 coefficient as data input, i.e. additional components of γ in Eq. (3) which the model $\boldsymbol{m}$ should fit. We assigned values to g_1^0 to the epochs of the knotpoints of our spline basis, that is every 60 years. For comparison with the snapshot models we preserved the fixed value of 30 μT. For our preferred new models, however, we used the

values of g_1^0 plotted in Fig. 6a. We set the values to those of GUFM (Jackson et al. , 2000) for the overlapping epochs back to 1600. The axial dipole moment gives the largest contribution to the total dipole moment. For the earlier epochs we therefore adopted linear approximations to the rate of change of the global dipole moment as determined from paleointensity data compiled by McElhinny and Senanayake (1982) for that time span. Our simple g_1^0-model now consists of three linear segments, one for every 1000 years, with this coefficient monotonically decreasing since 1000 B.C.Compared to the more recent study by Yang et al. (2000) of the global virtual dipole moment, we may have assumed slightly too high a dipole moment for the earliest few centuries. We chose the more linear older assumption in order to avoid overly complicated assumptions as we hope to include field intensity information in future models soon so that we will no longer need this constraint. Just as the directional data are weighted separately by a division by the uncertainty estimates, a constant multiplication weighting factor controls how closely the model fits the data input for the g_1^0 coefficient. Setting this factor to 10^{-2} ensures the close fit desired in this case of missing intensity information. The misfit between the artificial coefficient information and output model, however, is not considered in the determination of the RMS misfit discussed in Section 5.

4. A test with synthetic data

Compared to modern datasets the 24 sites used here provide very sparse coverage of the globe. Johnson and Constable (1998), based on Johnson and Constable (1997) showed by defining a sampling function how these few sites sample the field at the CMB and conclude that when all sites are present there is adequate coverage for sampling the radial magnetic field at the CMB between 40°S and 80°N. We used an additional approach to obtain a better notion of how well the limited dataset can represent a more complex structure by modelling synthetic data. We utilised the GUFM model (Jackson et al. , 2000), a continuous magnetic field model from historic and recent data, covering the 400 years between 1590 and 1990. The historical data prior to 1840 used for that model also consisted only of directional measurements along with an assumed continuing decrease of the dipole coefficient. We evaluated GUFM between 1690 and 1970 in twenty-nine 10 year intervals at exactly the 24 or fewer sites of our twenty-nine 100 year interval data of declination and inclination. We then modelled these synthetic records and compared the results with GUFM again. We used the constant axial dipole assumption again to see what difference if any that makes. Additionally we added normally distributed errors of the order as the estimated uncertainties of the data to the synthetic data prior to modelling.The results of this test are instructive for the evaluation of our subsequent models: As we hoped, we can reproduce the original GUFM quite well, even with errors added to the data. The choice of axial dipole constraint does not make a significant difference. Declination and inclination anomaly, the deviation of inclination from an axial dipole, do not show a lot of small scale structure, so our 24 sites for most epochs are sufficient to produce very similar models. For the radial component B_r at the CMB and the non-axial-dipole part of it, B_{rNAD}, GUFM shows more small scale structure in the more recent epochs, where an increasing number of reliable data were available. Naturally our few sites cannot resolve this small scale structure, but the general agreement particularly with the older, less structured epochs of GUFM is good. Fig. 2 shows the comparison of the original GUFM and a reproduction of the synthetic data with added errors, regularised just within the tolerance of those errors, for epoch 1970 when GUFM already shows a substantial amount of small-scale structure. The parameters used for this model are $\lambda = 10^{-7}\,\mathrm{nT}^{-2}$, $\tau = 10^{0}\,\mathrm{nT}^{-2}\,\mathrm{year}^4$, 35 iterations by which we obtain an RMS-misfit of 1.0 with a spatial norm of $19 \times 10^8\,\mathrm{nT}^2$ and a temporal norm of $28 \times 10^2\,\mathrm{nT}^{-2}\,\mathrm{year}^4$. The general agreement is good, only the small scale features of B_{rNAD} often cannot be represented too well. The reproduction lacks some of the flux lobes and others are clearly distorted by the under-sampling. The spatial as well as temporal lack of structure is also reflected by a comparison of the norms: the values of the reproduced model are significantly smaller than those of the original GUFM which are $35 \times 10^{12}\,\mathrm{nT}^2$ for the spatial and $6.8 \times 10^4\,\mathrm{nT}^{-2}\,\mathrm{year}^4$ for the temporal norm. However, the centres of the flux lobes that are present in the reproduced model are generally at the right positions and change according to the original model. We conclude that if we keep in mind the limitations

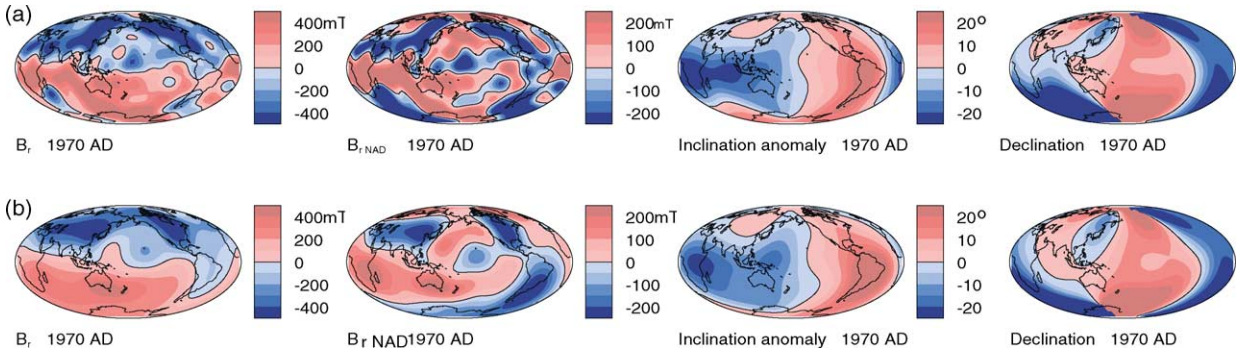

Fig. 2. GUFM (Jackson et al. , 2000) (a) and model from GUFM predictions at the 24 sites of Fig. 1 with normally distributed errors added (b). Radial component B_r and non-axial-dipole contribution B_{rNAD} at the CMB; inclination anomaly and declination at the Earth's surface with equal colour scheme.

of our sparse dataset, it can give us a good general representation of the field and secular variation at the CMB. Note, however, that this test can tell us nothing about the temporal resolution of the data. To test that we would need a realistic model of the field evolution over 3000 years with detailed spatial and temporal resolution. Despite efforts to develop one from statistics of the historical field, Hulot and LeMouël (1994) were only able to use information on time-scales of a tenth of the interval we are studying.

5. Comparison of different models

Solution of this inverse problem generated a whole suite of models obtained with different regularisation parameters. To present just one, we have to decide on a preferred model which we consider to be the closest representation of the real magnetic field. The models with the closest fit to the data are obtained with very low damping parameters. Such models, however, are not predominantly dipolar, either for older times or for the time overlapping with the GUFM model which clearly is dipole dominated. A predominantly dipolar structure of the magnetic field also is a sensible assumption for the whole time span of the last 3000 years. We therefore rule out all damping parameters that do not give dipole dominated models, i. e. very small ones and certain combinations of temporal and spatial damping. Very small root mean square (RMS) misfits can also be obtained if the temporal damping factor is small relative to the spatial one, but in those cases the coefficients show unreasonable high frequency oscillations in time. Comparisons confirm that the constraint on the dipole is mainly a scaling factor in our case and does not change the structure of models with equal parameters significantly. We therefore do not consider constant axial dipole models any further. To quantify the fit of different models to the data we look at the RMS misfit

$$\mathrm{RMS} = \sqrt{\frac{1}{N}\sum_{i=1}^{N}\left(\frac{x_i - \hat{x}_i}{\sigma_i}\right)^2} \tag{9}$$

between data x_i and model predictions $\hat{x}_i$, normalised by the uncertainties σ_i and the number of data N. The initial misfit between the data and a constant dipole starting model with $g_1^0 = -30\,\mu\mathrm{T}$ is 3.04. The values for the individual data epochs are listed in Table 1. Considering only dipole dominated models and ruling out models with oscillating coefficients the minimum normalised misfit at convergence reaches 0.99, which means that we can fit the data right to the tolerance of our uncertainty estimates. Although the misfit for the individual data epochs is close to 1 for many epochs, the extremes vary considerably: from as low as 0.18 for 1800 A.D. to 1.94 for 700 B.C. (see Table 1). This agrees with the results of Constable et al. (2000), who chose models with different levels of misfits for different epochs, arguing that they were not always able to fit their individual epoch models within the tolerance of the estimated errors without creating overly complicated models. Their misfits range from 1.00 to 2.93(Table 1), which gives an average of 1.62,

Table 1
Normalised RMS misfit between 100-year data and different models

Epoch A.D.	Number of data	Constant dipole	Rough model	Interm. model	Smooth model	Snapshot models[a]
−1000	31	3.74	0.81	1.03	1.42	1.87
−900	31	4.76	1.14	1.47	1.87	2.36
−800	31	5.33	1.38	1.82	2.20	2.51
−700	31	5.35	1.94	2.42	2.67	2.93
−600	33	4.58	1.21	1.61	2.00	2.14
−500	35	4.00	0.94	1.40	1.88	2.15
−400	35	3.12	0.92	1.26	1.65	1.79
−300	35	2.91	0.92	1.26	1.76	1.80
−200	35	3.32	0.93	1.27	1.61	1.55
−100	34	2.45	1.28	1.53	1.84	1.79
0	40	2.28	1.08	1.47	1.74	1.67
100	40	2.00	0.88	1.12	1.32	1.31
200	41	2.14	0.85	1.08	1.33	1.41
300	41	2.11	0.88	1.13	1.39	1.35
400	41	2.27	0.90	1.27	1.50	1.45
500	41	2.52	0.91	1.27	1.56	1.54
600	41	2.80	1.24	1.62	1.96	1.90
700	42	2.58	1.21	1.47	1.66	1.57
800	42	2.37	0.81	1.09	1.24	1.23
900	42	2.96	0.81	1.24	1.53	1.44
1000	45	3.29	0.86	1.17	1.46	1.39
1100	46	3.16	1.07	1.28	1.59	1.42
1200	46	2.72	0.97	1.20	1.47	1.38
1300	46	2.13	0.97	1.14	1.39	1.30
1400	45	2.06	0.73	1.03	1.37	1.27
1500	43	2.28	0.76	1.16	1.55	1.52
1600	41	2.50	0.73	0.93	1.23	1.00
1700	35	2.62	0.49	0.80	1.11	1.00
1800	28	3.26	0.18	0.39	0.78	1.00
Overall	–	3.04	0.99	1.30	1.61	1.62[b]

[a] Constable et al. (2000).
[b] Average of the individual models' misfits.

significantly larger than the estimated tolerance. For comparison we produced a model with a comparable misfit of 1.61 and the constant axial dipole constraint, the values are also listed in Table 1. Even here, the misfit for 1800 A.D. is smaller than 1.0.

We have to ask ourselves whether we are over-fitting the recent epochs if we obtain normalised misfits smaller than 1.0 for them, or whether those data are more accurate than estimated and we are under-fitting the older epochs when we are not obtaining fits close to their specified tolerance. A rigorous answer is not possible and we will describe the arguments used to choose a preferred model. Apart from the models with overall fit to the tolerance and comparable fit to the average misfit of the snapshot models, we also compared a model with an in-between misfit of 1.3. It gives a misfit of close to 1.0 for many of the epochs and is also listed in Table 1."Close to 1.0" of course is subjective and that model was chosen more or less arbitrarily from a range of models with misfits between 1.5 and 1.1. Models with very similar misfits do not show significant differences in their field predictions. Moreover, this is the average between the model with overall fit within the tolerance (RMS 1.0) and the model comparable in its misfit to the snapshot models, where only one epoch has a misfit smaller than 1.0. Table 2 gives an overview over the parameters that were used to obtain the three models with different misfits which we compare in the following.

We studied the different model predictions in comparison with the individual data series. The level to which individual series of declination and inclination

Table 2
Parmaters and norms of three models with different rms-misfits

RMS	λ (nT^{-2})	Spatial norm (nT^2)	τ (nT^{-2} year^4)	Temporal norm (nT^{-2} year^4)	g_1^0-constraint	Number of iterations
0.99	10^{-8}	56×10^9	10^{-3}	16×10^5	Decrease	35
1.30	10^{-7}	2×10^9	10^{-2}	18×10^4	Decrease	35
1.61	10^{-6}	13×10^9	10^0	55×10^2	Constant	35

are fit is quite different. It is not always true that for a larger RMS misfit the model shows a smoother variation in time than the data; the most extreme example is shown in Fig. 3. Generally data series which lie far away from the adjacent locations are fit better than some of the ones which are closer together. This is understandable, because we are looking for a spatially smooth model. If sites close to each other differ too much they cannot both be fit equally well without a lot of spatial structure. However, there are exceptions as shown in Fig. 3 for Hawaii, which lies far from any other site in the middle of the Pacific. Around 0 A.D.there is a bump in the model prediction for inclination that is not supported by the data. The fact that this bump decreases and almost vanishes for models with smaller misfit suggest that at least parts of the data are clearly under-fitted in models with larger misfit. In other cases, comparing data series and model seems to hint at dating problems with the data, as in the example of the archaeomagnetic site WUR (Western Europe) shown in Fig. 4a. The model shows the same behaviour as the data but with an apparent time shift of a few hundred years in the older epochs. In this case, however, this is not supported by declination (Fig. 4b) or one of the other European sites, so it is not clear what causes this effect. Iterative refinement of the model with an improved dataset should answer that question.

We compared our continuous models to the snapshot models by Constable et al. (2000) and, for the overlapping time interval, to GUFM (Jackson et al. , 2000). Fig. 5 shows, for epoch 1800 A.D., the snapshot model, two temporally continuous models with normalised misfits 1.30 and 0.99 and GUFM. A continuous model with comparable overall misfit of 1.61 gives very similar field predictions to the independent snapshot models for all components and all epochs. The models with smaller misfit and GUFM show more spatial structure. GUFM and the 3000-year models agree very well, particularly remembering that they originate from independent data sets: No historical data were used for the 3000 year models and no indirect data for GUFM. The data distribution is quite different. While the archaeo- and paleomagnetic sites are mostly located on the main continents, the historical data for the early epochs of GUFM mainly come from shipboard

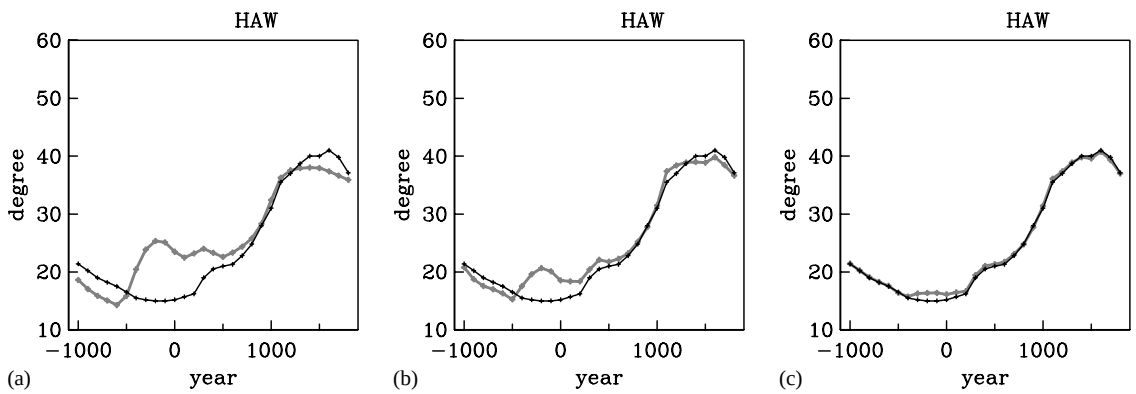

Fig. 3. Inclination data (thin black line) and model predictions (thick grey line) for Hawaii. Models with RMS-misfit (a) 1.61, (b) 1.30 and (c) 0.99.

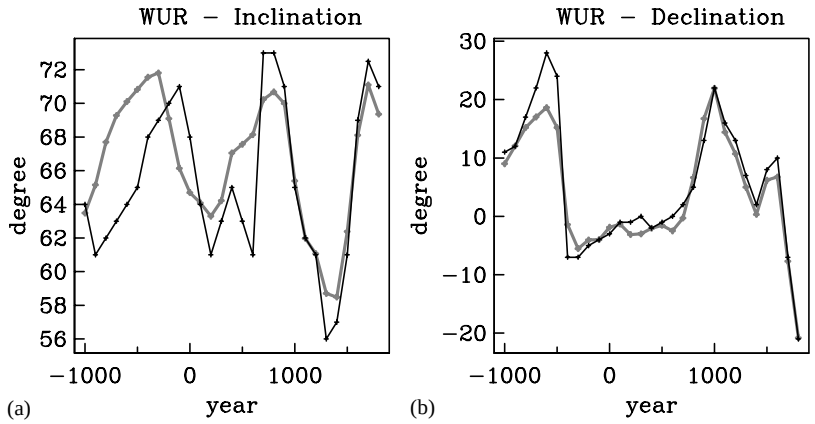

Fig. 4. Inclination (a) and declination (b) data (black) and model predictions (grey) for site WUR. Model with RMS misfit 1.30.

measurements for navigational purposes, and are distributed over the oceans. Moreover, the historical data are dominated by declination measurements, whereas declination has larger uncertainties or is completely missing in palaeomagnetic samples. However, if we believe GUFM to give a good representation of the actual field, our model with misfit 0.99 gives some additional structure which is most likely caused by data uncertainties. Constable et al. (2000) already argued that data uncertainties might be underestimated in PSVMOD1.0. On the other hand, for the model with overall misfit of 1.30 even the highly over-fitted epoch of 1800 A.D. with an RMS of 0.39 for the data of that epoch does not display more structure than

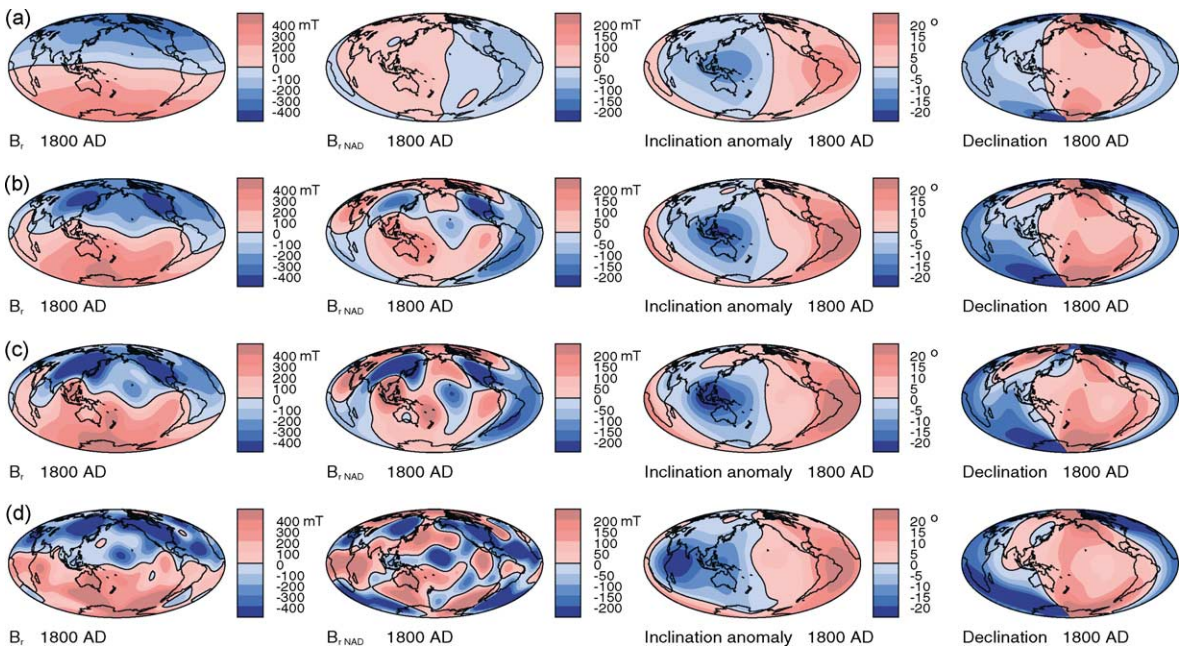

Fig. 5. Comparison of different geomagnetic field models for epoch 1800 A.D. Radial component B_r and non-axial-dipole part B_{rNAD} of radial component at the CMB, inclination anomaly and declination at the Earth's surface. (a) Snapshot model of Constable et al. (2000), (b) continuous model with normalised RMS misfit of 1.30, (c) continuous model with misfit 0.99, (d) GUFM (Jackson et al. , 2000).

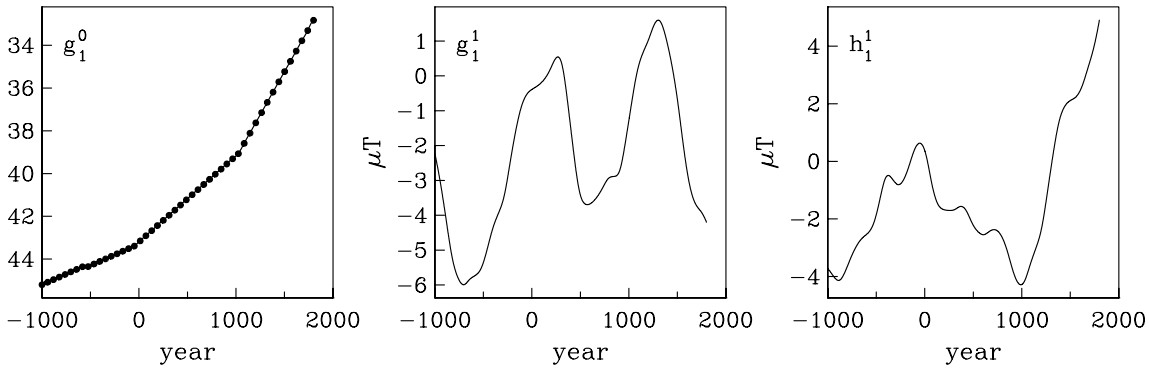

Fig. 6. Dipole coefficients of continuous model with misfit 1.30. For the axial dipole coefficient the dots are the preset values of the modelling constraint at the knotpoints of the spline basis.

GUFM, as Fig. 5 shows. So taking into account all the comparisons of this section, we decided to make the model with misfit 1.30 our preferred model, which shows as much structure as we believe is reliably required by the data. In Fig. 6 we show the behaviour of the dipole coefficients of that model through time, with the axial dipole coefficient meeting the imposed constraint. We name that model Continuous Archaeomagnetic and Lake Sediment Geomagnetic Model for the last 3k years (CALS3K.1) following the naming of Johnson and Constable (1998) for the averaged model from the same dataset. We introduce a version number 1 to leave room for planned improvements of the model by adding additional data, especially intensity information.

6. Discussion of CALS3K.1

CALS3K.1 essentially confirms the findings of Constable et al. (2000) from their individual snapshot models, but we observe some more detail in the structure of our preferred model. Moreover, the continuous representation allows a direct study of secular variation, and more clearly distinguishes between location changes and stationary growth and decay of structures. The lack of structure in the southern hemisphere must be attributed to the sparser data distribution there compared to the northern hemisphere. Fig. 7 gives some snapshots from the continuous model CALS3K.1. We do not want to repeat a display of a dense time series of snapshots as in the paper by Constable et al. (2000). Animations of the model give a much better idea of how the field evolves with time and and the reader is referred to our digital resources: movies from different viewpoints showing the continuous change and additional plots of snapshots every 100 years of the field and secular variation are available at http://www.mahi.ucsd.edu/cathy/Holocene/holocene.html. The whole package of files can also be downloaded from the Earthref digital archive at http://earthref.org/...

The radial component at the CMB shows two regions of strong negative flux over Asia and North America at 1000 B.C., similar to the two historically persistent lobes (Bloxham and Jackson , 1992). They show up again in the last centuries of the model, but are clearly not persistent throughout all the time. Strong negative flux occurs in parts of the northern Pacific about 200 B.C., 300 A.D. and 1200 A.D. The radial component is strongly dominated by the axial dipole contribution, the strength of which was assumed to account for the lack of intensity data. B_{rNAD}, the radial component after subtraction of the axial dipole contribution, shows more clearly the flux pattern deviating from a simple axial dipole. Those anomalies display complex changes over the three millennia. Both location changes and growth and decay of more or less stationary flux lobes can be seen. None of the flux lobes, however, are persistently stationary for the whole time span.

Inclination anomalies and declination predictions of CALS3K.1 also confirm those of the snapshot models, the only difference is one additional anomaly focus in each of those components in the early part of the

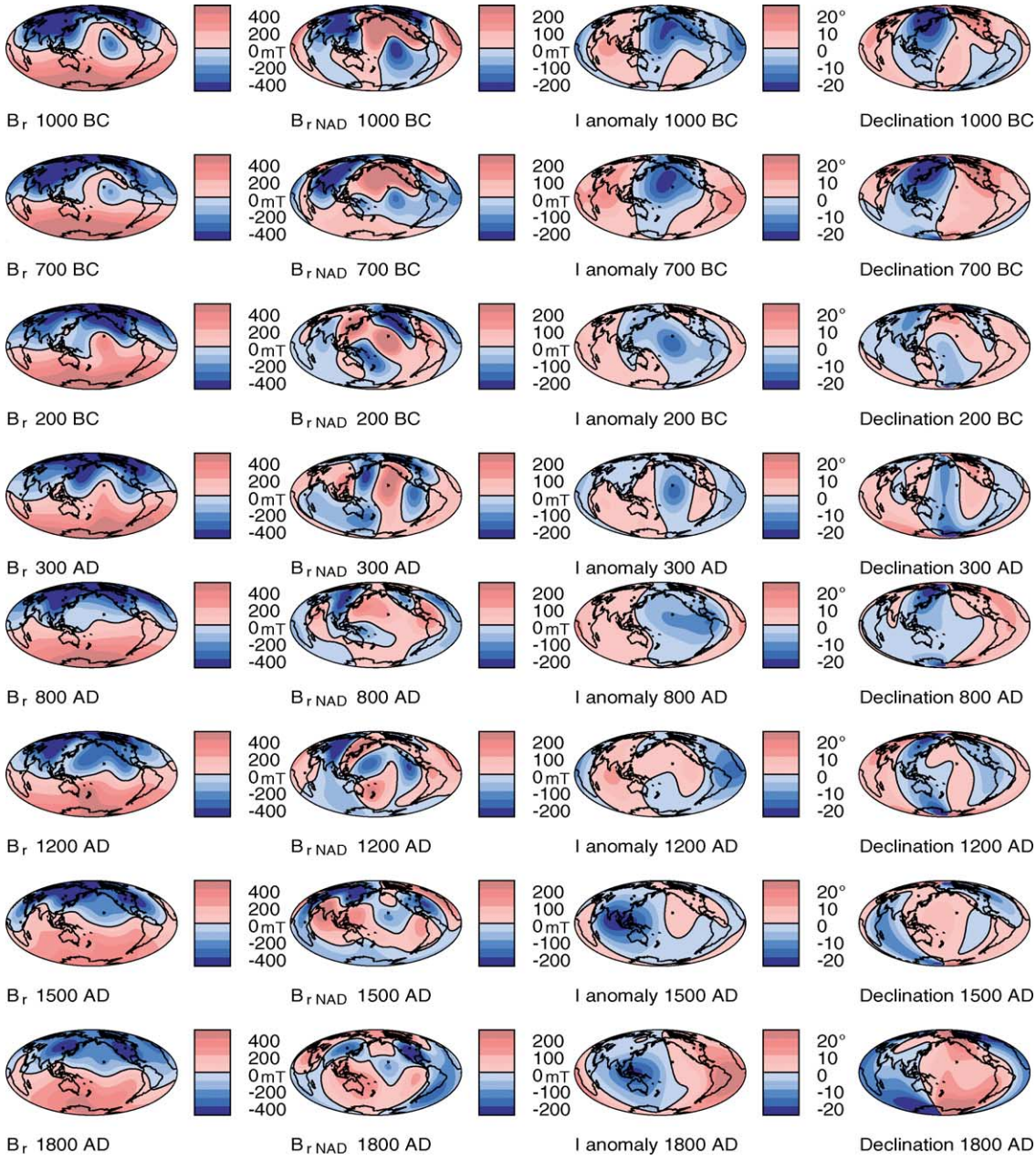

Fig. 7. Snapshots from the continuous model CALS3K.1. Columns show (1) B_r and (2) B_{rNAD} at the CMB, (3) inclination anomaly and (4) declination at the Earth's surface. Unequal time intervals were chosen to highlight some of the features described in the text. Inclination anomaly and declination have the same colour scale.Small black dots are the actual data sites available for each 100 year interval.

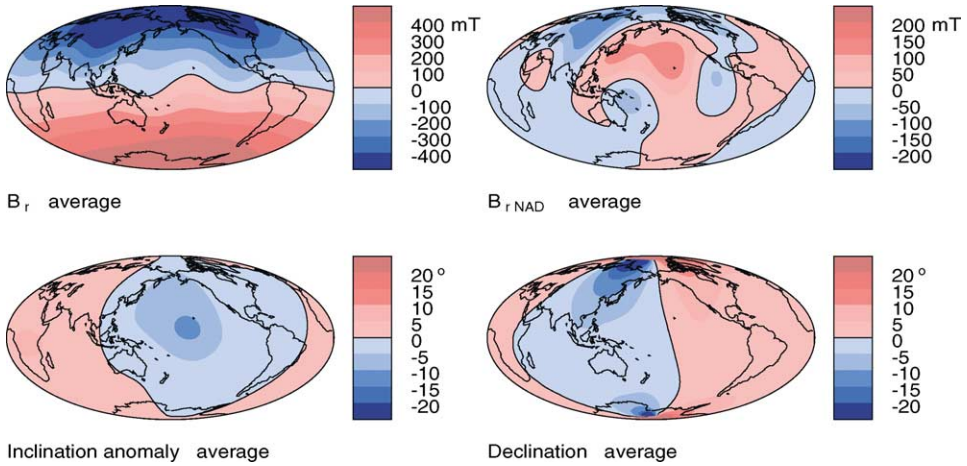

Fig. 8. Averages for B_r and B_{rNAD} at the CMB and declination and inclination anomaly at the Earth's surface.

model. In addition to the initial large negative inclination anomaly in the central Pacific region and the positive one centred in the Indian ocean, there appears a second negative anomaly over the Atlantic from 1000 B.C. to 850 B.C. which gives way to a second positive focus lasting to about 600 B.C. Declination naturally is strongest close to the poles. The initial simple two hemisphere pattern of negative declination centred from eastern Asia to south of Australia and positive declination centred on the Atlantic is disturbed by

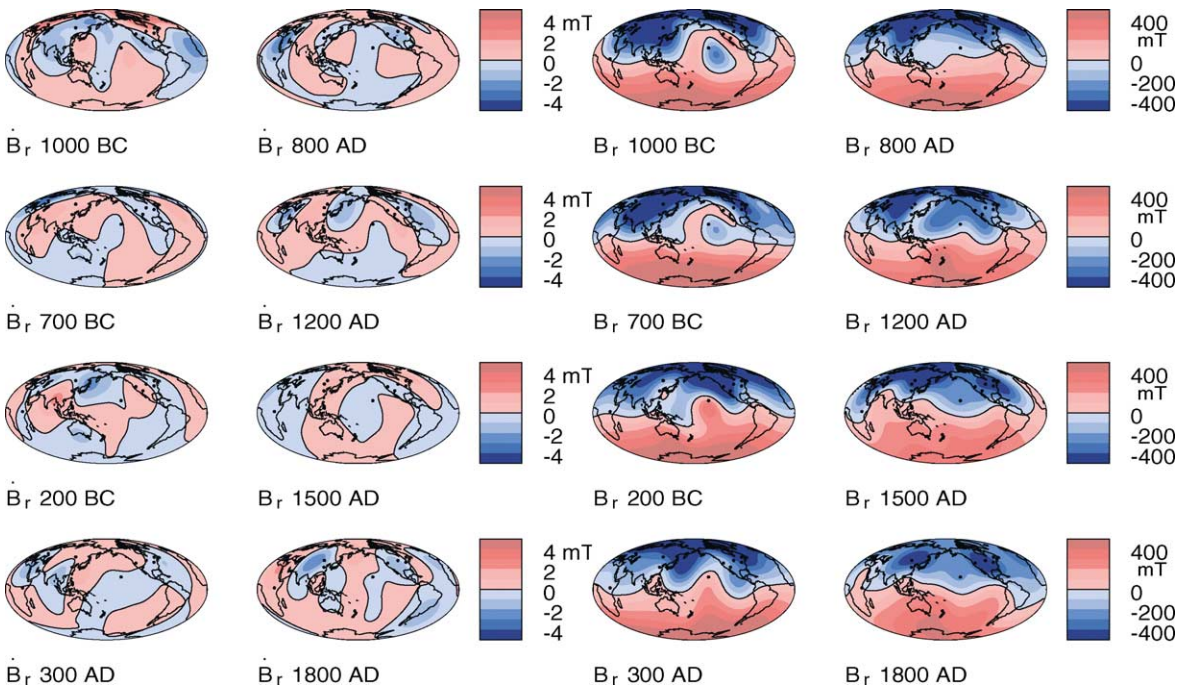

Fig. 9. Snapshots of secular variation of the radial component $\dot{B}_r$ at the CMB for the same epochs as shown in Fig. 7. The B_r plots from that figure are repeated on the right for comparison.

another area of negative declination stretching south from South America. However, this feature vanishes by 600 B.C. and might be spurious, as it lies far from any of the data sites available for those early epochs.

Recent (Hulot et al. , 2002) and historical (Bloxham et al. , 1989) observations of low secular variation in the Pacific region compared to the rest of the world led us to look for regional distinctions in our model, too. With the amount of change displayed in the model predictions, however, it often is hard to decide which impressions are reliable. At several intervals we observe a third negative flux lobe over the European region, but a similarly strong feature never seems to appear over the central Pacific region. Looking at the animated evolution of the field, in particular the non-axial-dipole radial component, one might also get the impression that there are regions where spatial movement of anomalies dominates and others where growth and decay of more stationary patches prevails. However, all these observations are hard to quantify and they also might be influenced by the data distribution. A lot of sites are contributing to the central northern region of the European hemisphere. In contrast, when looking at the Pacific region centred at longitude 180°, areas of denser coverage lie only near the border of that hemisphere.

Time averages might reveal systematic regional differences. An average of CALS3K.1, obtained as the sum of the annual coefficients divided by the total number of years, differs only slightly from the average of the individual 100-year epoch snapshot models. Fig. 8 shows the averaged B_r, B_{rNAD}, Declination and Inclination anomaly.

The Asian flux lobe dominates B_r in the 1000 B.C. to 1800 A.D. time-averaged field, but a second, weaker lobe over North America is also present. Remember again that the lack of structure in the southern hemisphere is most likely due to the scarce data coverage there. B_{rNAD} additionally shows a strong positive

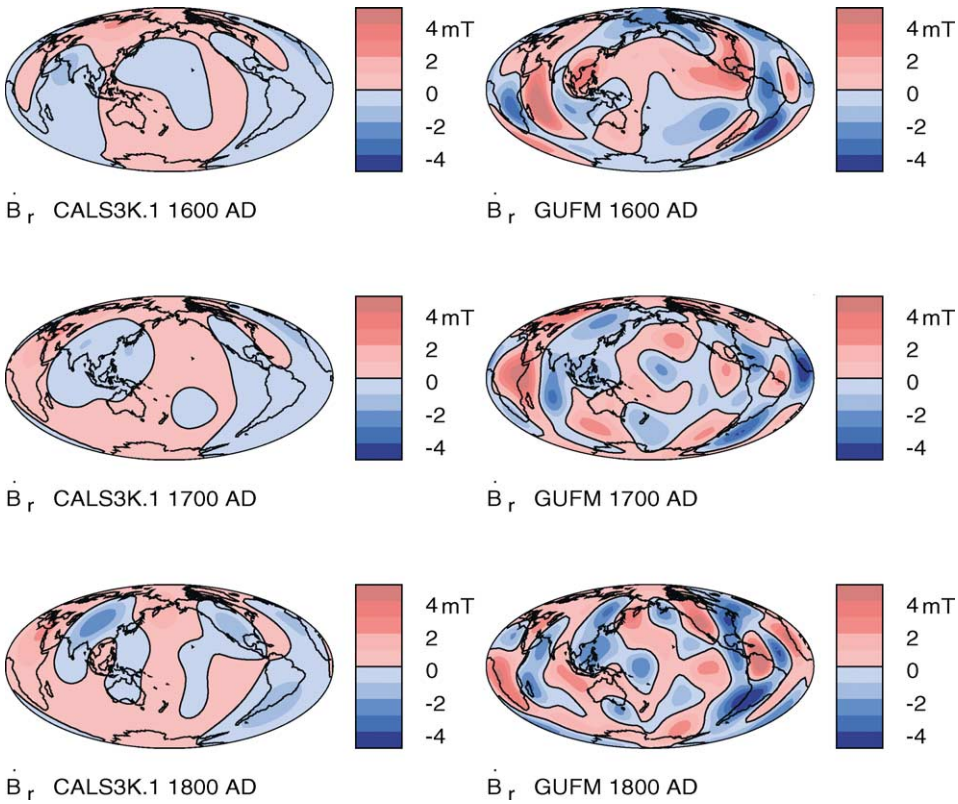

Fig. 10. Comparison of secular variation $\dot{B}_r$ from CALS3K.1 (left) and GUFM (right) for three epochs. GUFM shows significantly more small-scale structure.

anomaly with two foci in the Pacific region. Average declination and inclination anomaly at the Earth's surface show quite simple patterns with one large positive and one negative sector each. The negative inclination anomaly covers a sector from Australia and eastern Asia over the Americas well into the northern Atlantic with a strong focus over the central Pacific. The focus of the positive anomaly is weaker and located over central Africa. In declination the negative sector covers the region from the Indian Ocean eastward to the middle of the Pacific. Two foci per sector are located near the poles, respectively, reflecting the geometric influence of increasing latitude on declination.

Continuous models like CALS3K.1 also allow the direct investigation of secular variation by looking at the temporal derivative of the coefficients. In Fig. 9 we show secular variation snapshots for $\dot{B}_r$ for the equivalent epochs of the model snapshots in Fig. 7. A complete set of 100 year snapshots and a movie are also available in the Earthref digital archive. A large amount of change is visible, but CALS3K.1 shows significantly less small scale secular variation structure than GUFM, as shown for three epochs in Fig. 10. These comparisons show general agreement of larger areas of positive or negative secular variation, respectively for 1700 A.D.and more or less for 1800 A.D., but for 1600 A.D. the pattern looks quite different. The reliability of secular variation of global models at the CMB is controversial even for recent models. We cannot answer the question whether the differences in the older epochs are due to generally unreliable secular variation predictions of the models or simply to

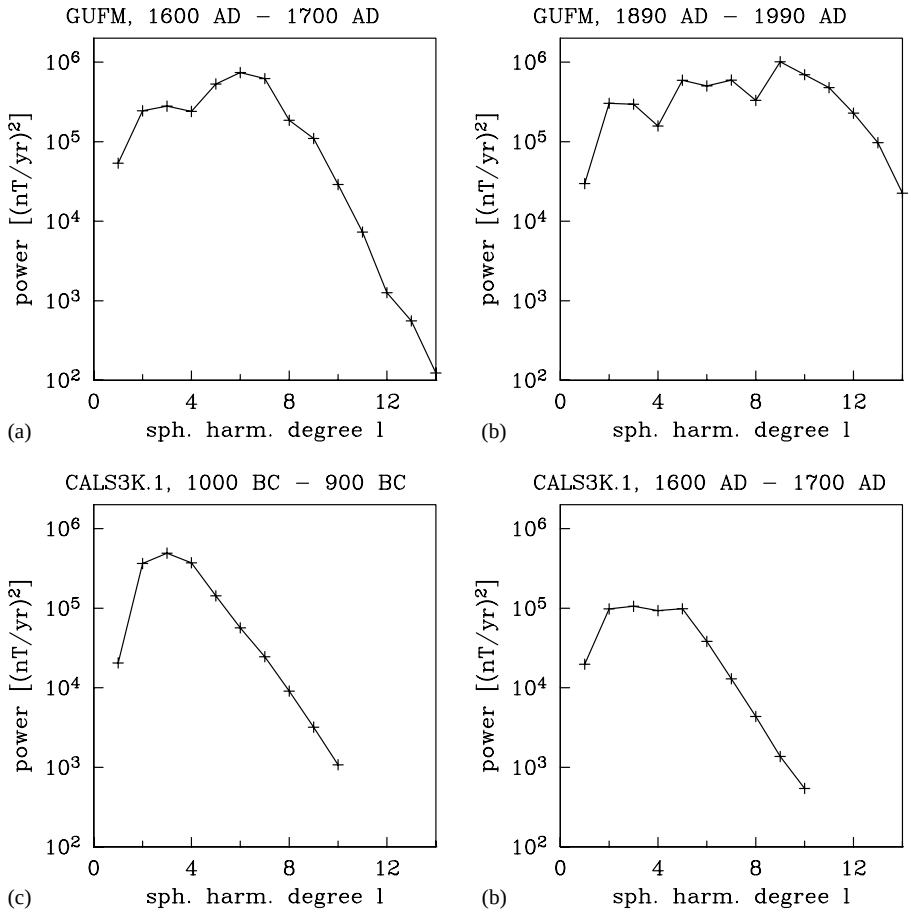

Fig. 11. Power spectra of 100 year averages of secular variation at the CMB. Examples from early and recent time intervals of the GUFM and CALS3K.1 models.

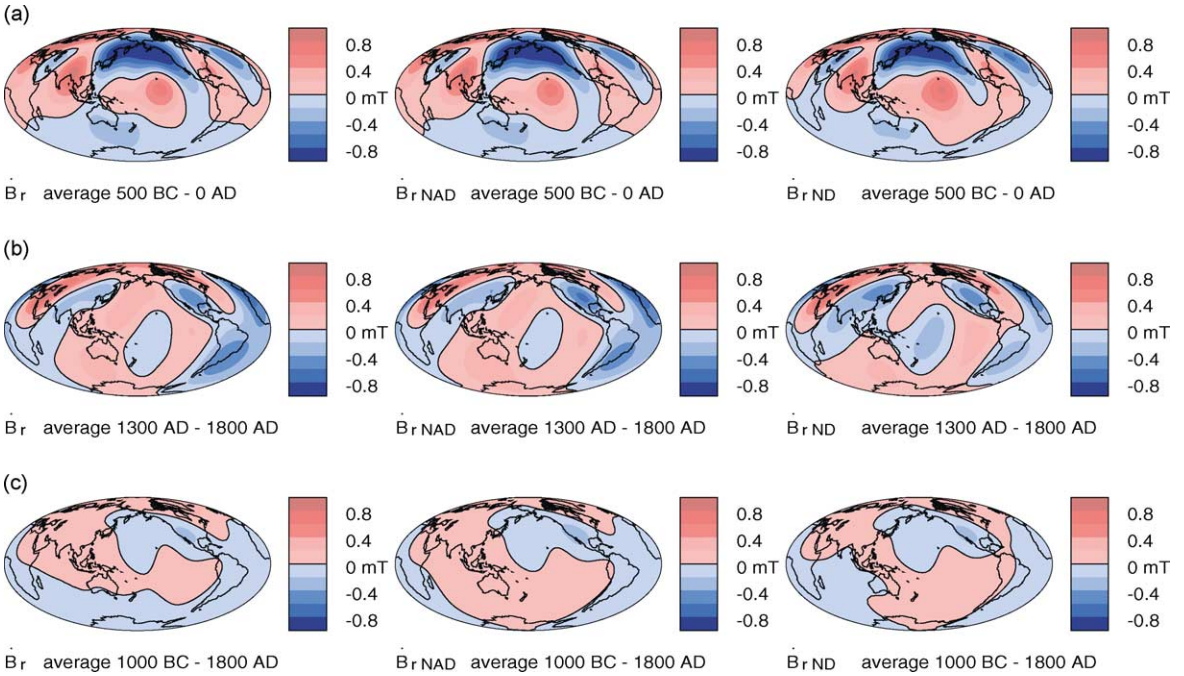

Fig. 12. Averaged secular variation for the time intervals 500 B.C.–0 A.D. (a), 1300 A.D.–1800 A.D. (b) and the whole 3 millennia (c). Radial component $\dot{B}_r$, non-axial-dipole radial component $\dot{B}_{rNAD}$ and non-dipole component $\dot{B}_{rND}$ at the CMB.

significant differences in data distribution of sparse data sets. The agreement in the comparison of the youngest epochs of CALS3K.1 with GUFM, however, led us to present the secular variation predictions of CALS3K.1 and encourage further investigations about the reliability of those predictions.

A comparison of spherical harmonic power spectra (Lowes , 1974; Mauersberger , 1956) of secular variation at the CMB for 100 year averages reveals that for GUFM the power in secular variation is mainly concentrated around degrees 5–7 for the earlier centuries and 5–10 for the more recent ones (Fig. 11a and b). In contrast, for our model secular variation power is mainly concentrated in degrees 2–5 for the whole time span (Fig. 11c and d). These power concentrations again reflect the spatial resolution of the models. It also means that secular variation is dominated by changes of the non-dipole contribution, which is confirmed when comparing predictions of $\dot{B}_{rNAD}$ or $\dot{B}_{rND}$, the radial component after subtraction of the complete dipole contribution, to those of $\dot{B}_r$. The plots look almost the same, as we demonstrate in Fig. 12. The comparison in Fig. 9 suggests that areas of strong secular variation are often associated with regions where B_r is strong.

It is easier to interpret the change going on when looking at averages of secular variation over longer time intervals. In Fig. 12 we show two examples of 500 year averages of annual secular variation, and the overall average for our model. Note the different colour levels in comparison to Fig. 9. Most of the observed secular variation averages out significantly (Fig. 12c). The historically low secular variation in the Pacific region is supported by CALS3K.1 (Fig. 12b), but that is only a short-lived phenomenon and at earlier times significant amounts of secular variation can be observed in that area, too (Fig. 12a).

7. Conclusions and outlook

With CALS3K.1 we presented a first attempt at a temporally continuous global geomagnetic field model for the last 3000 years. The minimum structure constraint in both space and time used in the modelling provides a highly improved reliability of

temporal change compared to individual snapshot models. The regularisation tries to preserve smooth structure through time so that the influence of changes in data distribution is reduced. The evolution of both the geomagnetic field and secular variation can be studied for any time within the interval 1000 B.C. to 1800 A.D.CALS3K.1 confirms the main results of Constable et al. (2000) while giving slightly more detailed features. The average of CALS3K.1 shows both of the northern hemisphere flux lobes which appear persistent in historical models and are present in several paleomagnetic time-averaged models.

The dataset that we used consists of values in 100 year intervals taken from time series which have been smoothed to different degrees. Smooth time series, however, are not required for the kind of modelling we have described. A model from the original data with improved resolution is the ultimate goal of our work. The archaeomagnetic data for each of our locations generally are not from a single site but sample results from a larger region reduced to one location. For lake sediments the temporal resolution of the time series often is better than 100 years (although an averaging over some decades can be inherent to the kind of magnetisation studied here), and for the archaeomagnetic data the intervals are uneven. We believe CALS3K.1 to give a reliable general representation of secular variation and magnetic flux at the CMB, but it should by no means be regarded as a definitive, highly accurate representation of the actual geomagnetic field of that time. Improving the model, however, must be an iterative process. The modelling becomes less robust when the data are more scattered and data errors are large. We have no absolute reference to check the quality of data, but must rely on regional consistency arguments. CALS3K.1 can be used to compare archaeo- and paleomagnetic time series to its predictions. For areas like North America, Europe, the north-east of Asia or the southern Australia region with good data coverage we believe it to give quite reliable predictions, meaning that data that disagree with model predictions should be studied very critically as they clearly would not agree with the general field evolution in that region. However, keep in mind the discussion about judging dating problems in Section 5. In regions where only sparse data went into the model, one should also view the model very critically. Only including additional data in an improved model can answer the question of whether a different field evolution in those regions might not be compatible with an as-smooth-as-possible global representation and the existing data.

Acknowledgements

We thank Richard Holme for useful discussions about the modelling method. We also wish to thank David Gubbins and Gauthier Hulot for constructive reviews of the original manuscript. All the global field charts were created with the programs “magmap” and “color” by Robert L. Parker. Large parts of this study were completed while MK was financially supported by a Feodor-Lynen fellowship of Alexander von Humboldt-Foundation at Scripps Institution of Oceanography. Further support for this work was provided by funding from NSF grant EAR 0112290.

References

Bloxham, J., Gubbins, D., 1987. Thermal core-mantle interactions. Nature 325, 511–513.

Bloxham, J., Gubbins, D., Jackson, A., 1989. Geomagnetic secular variation. Philos. Trans. R. Soc. London Ser. A 92, 415–502.

Bloxham, J., Jackson, A., 1992. Time-dependent mapping of the magnetic field at the core-mantle boundary. J. Geophys. Res. 97, 19537–19563.

Carlut, J., Courtillot, V., 1998. How complex is the time-averaged geomagnetic field over the last 5 million years. Geohpys. J. Int. 134, 527–544.

Clark, R.M., 1975. A calibration curve for radiocarbon dates. Antiquity 49, 251–266.

Constable, C.G., Johnson, C.L., Lund, S.P., 2000. Global geomagnetic field models for the past 3000 years: transient or permanent flux lobes, Phil. Trans. R. Soc. Lond. A 358, 991–1008.

Constable, S.C., Parker, R.L., Constable, C.G., 1987. Occam’s inversion: a practical algorithm for generating smooth models from electromagnetic sounding data. Geophys 52, 289–300.

de Boor, C., 1978. A Practical Guide to Splines. Springer, New York, 1978.

Daly, L., Le Goff, M., 1996. An updated and homogeneous world secular variation database. Part 1. Smoothing of the archeomagnetic results. Phys. Earth Planet. Interiors 93, 159–190.

Gubbins, D., 1975. Can the Earth’s magnetic field be sustained by core oscillations? Geophys. Res. Lett. 2, 409–412.

Gubbins, D., 1983. Geomagnetic field analysis. Part I. Stochastic inversion. Geophys. J. R. Astron. Soc. 73, 641–652.

Gubbins, D., Bloxham, J., 1985. Geomagnetic field ananlysis. Part III. Magnetic fields on the core-mantle boundary. Geophys. J. R. Astron. Soc. 80, 695–713.

Gubbins, D., Richards, M., 1986. Coupling of the core dynamo and mantle-thermal or topographic. Geophys. Res. Lett. 325, 1521–1524.

Hatakeyama, T., Kono, M., 2002. Geomagnetic field model for the last 5 Myr: time-averaged field and secular variation. Phys. Earth Planet. Interiors 133, 181–215.

Hongre, L., Hulot, G., Khokhlov, A., 1998. An analysis of the geomagnetic field over the past 2000 years. Phys. Earth Planet. Interiors 106, 311–335.

Hulot, G., Eymin, C., Langlais, B., Mandea, M., Olsen, N., 2002. Small-scale structure of the geodynamo inferred from Oersted and MAGSAT satellite data. Nature 416, 620–623.

Hulot, G., Khokhlov, A., LeMouël, J.L., 1997. Uniqueness of mainly dipolar magnetic fields recovered from directional data. Geophys. J. Int. 129, 347–354.

Hulot, G., LeMouël, J.L., 1994. A statistical approach to the Earth's main magnetic field. Phys. Earth Planet. Interiors 82, 167–183.

Jackson, A., Jonkers, A.R.T., Walker, M.R., 2000. Four centuries of geomagnetic secular variation from historical records. Phil. Trans. R. Soc. Lond. A 358, 957–990.

Johnson, C.L., Constable, C.G., 1997. The time-averaged geomagnetic field: global and regional biases for 0-5 Ma. Geohpys. J. Int. 131, 643–666.

Johnson, C.L., Constable, C.G., 1998. Persistently anomalous Pacific geomagnetic fields. Geohpys. Res. Lett. 25, 1011–1014.

Kelly, P., Gubbins, D., 1997. The geomagnetic field over the past 5 Myr. Geophys. J. Int. 128, 315–330.

Lowes, F.J., 1974. Spatial power spectrum of the main geomagnetic field, and extrapolation to the core. Geophys. J. R. Astron. Soc. 36, 717–730.

Mandea, M., Macmillan, S., 2000. International geomagnetic reference field, the eighth generation. Earth Planets Space 52, 1119–1124.

Mauersberger, P., 1956. Das Mittel der Energiedichte des geomagnetischen Hauptfeldes an der Erdoberfläche und seine säkulare Änderung. Gerlands Beitr. Geophys. 65, 207–215.

McElhinny, M.W., McFadden, P.L., Merrill, R.T., 1996. The time averaged paleomagnetic field 0–5 Ma. J. Geophys. Res. 101, 25007–25027.

McElhinny, M.W., Senanayake, W.E., 1982. Variations in the geomagnetic dipole. Part I. The past 50 000 years. J. Geomag. Geoelectr. 34, 39–51.

Merrill, R.T., McElhinny, M.W., McFadden, P.L., 1996. The Magnetic Field of the Earth. Academic Press, San Diego.

Parker, R.L., 1994. Geophysical Inverse Theory. Princeton University Press, 1994.

Roberts, P.H., Scott, S., 1965. On the analysis of the secular variation. Part 1. A hydromagnetic constraint: Theory. J. Geomag. Geoelectr. 17, 137–151.

Sabaka, T.J., Langel, R.A., Baldwin, R.T., Conrad, J.A., 1997. The geomagnetic field 1900–1995, including the large-scale field from magnetospheric sources, and the NASA candidate models for the 1995 revision of the IGRF. J. Geomag. Geoelectr. 49, 157–206.

Sabaka, T.J., Olsen, N., Langel, R.A., 2002. A comprehensive model of the quiet-time, near-earth magnetic field: phase 3. Geohpys. J. Int. 151, 32–68.

Schneider, D.A., Kent, D.V., 1990. The time-averaged paleomagnetic field. Rev. Geohpys. 28, 71–96.

Stuiver, M., Reimer, P.J., 1993. Extended ^{14}C data base and revised CALIB 3.0 ^{14}C age calibration program. Radiocarbon 35, 215–230.

Stuiver, M., Reimer, P.J., Bard, E., Beck, J.W., Burr, G.S., Hughen, K.A., Kromer, B., McCormac, G., van der Plicht, J., Spurk, M., 1998. INTCAL98 radiocarbon age calibration, 24,000-0 cal BP. Radiocarbon 40, 1041–1083.

Whaler, K.A., Gubbins, D., 1981. Spherical harmonic analysis of the geomagnetic field: an example of a linear inverse problem. Geophys. J. R. Astron. Soc. 65, 645–693.

Yang, S., Odah, H., Shaw, J., 2000. Variations in the geomagnetic dipole moment over the last 12,000 years. Geophys. J. Int. 140, 158–162.